UGGT1/2-mediated reglucosylation of *N*-glycan competes with ER-associated degradation of unstable and misfolded glycoproteins

Satoshi Ninagawa[1, 2*#], Masaki Matsuo[2#], Deng Ying[3#], Shinya Aso[3], Kazutoshi Matsushita[3], Akane Fueki[2], Shunsuke Saito[3], Koshi Imami[4], Yasuhiko Kizuka[5], Tetsushi Sakuma[6], Takashi Yamamoto[6], Hirokazu Yagi[7,8], Koichi Kato[7, 8, 9] and Kazutoshi Mori[3*]

[1] Biosignal Research center, KOBE University, Kobe 657-8501, Japan
[2] Department of Bioresource Science, Graduate School of Agricultural Science, Kobe University, Kobe 657-8501, Japan
[3] Department of Biophysics, Graduate School of Science, Kyoto University, Kyoto 606-8502, Japan
[4] Proteome Homeostasis Research Unit, RIKEN Center for Integrative Medical Sciences, Yokohama, Kanagawa 230-0045, Japan
[5] Laboratory of Glycobiochemistry, Institute for Glyco-core Research (iGCORE), Gifu University, Gifu 501-1193, Japan
[6] Division of Integrated Sciences for Life, Graduate School of Integrated Sciences for Life, Hiroshima University, Hiroshima 739-8526, Japan
[7] Graduate School of Pharmaceutical Sciences, Nagoya City University, Nagoya 467-8603, Japan
[8] Exploratory Research Center on Life and Living Systems (ExCELLS), National Institutes of Natural Sciences, Okazaki 444-0864, Japan
[9] Institute for Molecular Science (IMS), National Institutes of Natural Sciences, Okazaki 444-0864, Japan

Running Title: UGGTs prevent glycoprotein ERAD

Key Words: ER protein quality control, Protein folding and degradation

Abbreviations: UGGT1, UDP-glucose glycoprotein glucosyltransferase 1; ER, endoplasmic reticulum; CNX, Calnexin; CRT, Calreticulin; gpERAD, glycoprotein ER-associated degradation; non-gpERAD, non-glycoprotein ER-associated degradation; EDEM, ER degradation enhancing α-mannosidase-like protein; ATF6, Activating transcription factor 6; ATF4, Activating transcription factor 4; PDI, Protein disulfide isomerase; GlcNAc, *N*-acetylglucosamines; TXNDC11, Thioredoxin domain-containing protein 11; WT, wild type; DKO, double knockout; TKO, triple knockout; Puro, puromycin; Hygro, hygromycin; BiP, immunoglobulin heavy chain binding protein; EMC1, ER membrane protein complex subunit 1; EndoH, endoglycosidase H; DNJ, 1-deoxynojirimycin; CHX, cycloheximide; ERSE, ER stress responsive element; UPRE, unfolded protein response element; CRISPR, Clustered regularly interspaced short palindromic repeats; TALEN, Transcription activator-like effector nuclease; BLAST, Basic Local Alignment Search Tool; PQQ, pyrrolo-quinoline quinone; Tg, thapsigargin; XBP1, X-box binding protein 1; PERK, Protein kinase R (PKR)-like endoplasmic reticulum kinase; IRE1, Inositol-requiring enzyme 1; GAPDH, Glyceraldehyde-3-phosphate dehydrogenase; HA, Hemagglutinin; A1AT, Alpha-1 antitrypsin; NHK, null hong kong; EPO, Erythropoietin; SDS, sodium dodecyl sulfate

ABSTRACT

Here we investigated how the fate (folding versus degradation) of glycoproteins is determined in the endoplasmic reticulum (ER). Monoglucosylated glycoproteins are recognized by lectin chaperones to facilitate their folding, whereas glycoproteins with well-trimmed mannoses are subjected to glycoprotein ER-associated degradation (gpERAD). Previously we elucidated how mannoses are trimmed by EDEM family members (George et al., 2020, 2021 eLife). Though reglucosylation by UGGTs (UGGT1 and UGGT2) was reported to have no effect on substrate degradation, here, we directly test this using genetically disrupted UGGTs. Strikingly, the results showed that UGGTs (mainly UGGT1) delayed the degradation of misfolded substrates and unstable glycoproteins including ATF6α. An experiment with a point mutant of UGGT1 indicated that the glucosylation activity of UGGT was required for the inhibition of early glycoprotein degradation. We further demonstrated the physiological importance of UGGT, since ATF6 cannot function properly without UGGTs. The fate of glycoproteins is determined by a tug-of-war between structure formation by UGGTs and degradation by EDEMs. Thus, our work strongly suggests that UGGTs are central factors in ER protein quality control via regulation of both glycoprotein folding and degradation.

INTRODUCTION

The endoplasmic reticulum (ER) plays an essential role in the cell as the site of biosynthesis of approximately one third of all proteins. Membrane and secretory proteins, after being newly synthesized on ribosomes attached to the ER membrane, are translocated to the ER in a translation-coupled manner (Brodsky and Skach, 2011). Post-translational modifications of proteins occurring in the ER include disulfide bond formation mediated by PDI (protein disulfide isomerase) family members and *N*-linked glycosylation of Asn in the consensus sequence consisting of Asn-X-Ser/Thr (X≠Pro). *N*-Glycan modifying a large number of proteins that enter the ER is converted from oligomannose type to complex type in the Golgi and is deeply involved in biological phenomena inside and outside the cell.

The structure of *N*-glycans plays a key role in protein folding and degradation in the ER (Berner et al., 2018; Ninagawa et al., 2020a). The *N*-glycan added to nascent proteins is composed of three glucoses, nine mannoses, and two *N*-acetylglucosamines (GlcNAc), and termed $Glc_3Man_9GlcNAc_2$ (G3M9), which is processed to GM9 by the action of glucosidase I and glucosidase II. Calnexin (CNX) and calreticulin (CRT) recognize glycoproteins with GM9 to facilitate productive folding (Lamriben et al., 2016) and then the last glucose is removed by glucosidase II. If glycoproteins with M9 attain their tertiary structure, they move on to the next compartment of the secretory pathway (Ninagawa et al., 2020a). If the protein portion does not form a proper structure, UDP-glucose glycoprotein glucosyltransferses (UGGTs: UGGT1 and UGGT2) re-add glucose to the glycoprotein (reglucosylation) for recognition by CNX/CRT to facilitate protein folding, collectively referred to as the "CNX/CRT" cycle (Lamriben et al., 2016; Sun and Brodsky, 2019). UGGT1 promotes substrate solubility (Ferris et al., 2013) and prefers

proteins with exposed hydrophobic regions to folded proteins (Caramelo et al., 2004; Sousa and Parodi, 1995). UGGT1 has a homologue, UGGT2, whose glucosyltransferase activity is weaker than that of human UGGT1 (Ito et al., 2020; Takeda et al., 2014).

If glycoproteins with M9 are not folded correctly within a certain period, mannose residues are trimmed from M9 first by EDEM2-S-S-TXNDC11 complex to M8B (George et al., 2020; Ninagawa et al., 2014) and then by EDEM3/1 to M7A, M6 and M5 exposing α1,6-bonded mannose on the glycoproteins (George et al., 2021; Hirao et al., 2006; Ninagawa et al., 2014), which are recognized by the OS9 or XTP3B lectins for degradation (van der Goot et al., 2018). They are recruited to the HRD1-SEL1L complex on the ER membrane, retrotranslocated back to the cytosol, and degraded via the ubiquitin-proteasome system (Fig. 1A). The series of these processes are collectively designated glycoprotein ER-associated degradation (gpERAD) (Ninagawa et al., 2020a; Smith et al., 2011).

However, how the fate of glycoprotein (folding versus degradation) is determined is not clearly understood, and remains one of the biggest issues in the field of ER protein quality control. One of the key enzymes for this appeared to be UGGTs. UGGTs have been shown to contribute to glycoprotein folding through its reglucosylation activity (Helenius and Aebi, 2004; Pearse et al., 2010; Sousa et al., 1992; Tessier et al., 2000), but did not appear to be related to ERAD, because it was previously reported that the presence of one glucose in the A branch of *N*-glycans was not involved in timing for substrate degradation (Tannous et al., 2015). MI8-5 Chinese hamster ovary cells are deficient in the dolichol-P-glucose–dependent glycosyltransferase termed Alg6, and therefore produce only glycoproteins with *N*-glycans lacking glucoses (M9). In these cells, *N*-glycans with one glucose are produced only by the action of UGGTs. In the experiment,

the monoglucosylated state is maintained by treatment with the glucosidase inhibitor 1-deoxynojirimycin (DNJ). It was found that such trapping of glycoproteins in a monoglucosylated state did not affect their rate of disposal, while trapping of UGGT1 substrates for secretion in a monoglucosylated state with DNJ delayed their efflux from the ER. The degradation selection process seemed to progress in a dominant manner that was independent of glucosylation state of A-branch on the substrate glycans.

We consider that it has not been directly examined whether UGGTs-mediated reglucosylation of *N*-glycan is involved in degradation of glycoproteins in the ER. Here, we generated UGGT1-KO, UGGT2-KO and UGGT-double KO (DKO) cell lines to investigate this involvement. Unexpectedly, it was revealed that degradation of misfolded and unstable proteins was markedly accelerated in these KO cells. Our work thus dramatically demonstrates the importance of UGGTs in ER protein quality control via involvement in protein degradation as well as protein folding in the ER.

RESULTS & DISCUSSION

Generation of knockout cell lines of UGGTs

To explore the roles of UGGT1 and UGGT2 in ERAD, UGGT1-KO, UGGT2-KO and UGGT-DKO cell lines were generated in HCT116 diploid cells derived from human colonic carcinoma using Clustered Regularly Interspaced Short Palindromic Repeats (CRISPR)-Cas9. Gene disruptions of UGGT1 and UGGT2 were confirmed at the genome, mRNA and protein level (Figure 1-figure supplement 1A-K). The growth rate of the KO cell population was not significantly altered (Figure 1-figure supplement 1L).

Previously, the protein level of UGGT2 was estimated to be 4% relative to that of UGGT1 in HeLa cells (Adams et al., 2020; Itzhak et al., 2016). In our hands, the protein expression levels of UGGT2 in HCT116 and HeLa cells were found to be approximately 6.9% and 29.8% of that of UGGT1, respectively, as estimated by transfection of UGGT1-Myc3 and UGGT2-Myc3 (Figure 1-figure supplement 2A). Immunoblotting showed that ER stress marker proteins BiP, XBP1(S) and ATF4 were not induced in UGGT1-KO, UGGT2-KO or UGGT-DKO cells (Figure 1-figure supplement 2B). Both UGGT1 and UGGT2 are modified with several *N*-glycans, as indicated by their sensitivity to treatment with EndoH, which cleaves oligomannose-type *N*-glycans localized in the ER (Figure 1-figure supplement 2C).

In UGGT1-KO and UGGT-DKO cells but not in UGGT2-KO cells, the secretion efficiency of α1-antitrypsin (A1AT) and erythropoietin (EPO) determined by pulse-chase experiments using ^{35}S was decreased (Figure 1-figure supplement 2DE). In UGGTs-KO cells, maturation of hemagglutinin (HA) from oligomannose type to complex type was delayed, as reported previously (Figure 1-figure supplement 2F) (Hung et al.,

2022). These results confirmed the establishment of KO cells for UGGTs and show the expected phenotype being involved in the maturation of nascent polypeptides.

Effect of UGGT1/2 knockout on ERAD

We then examined the effect of UGGT1/2 knockout on ERAD. We previously showed that ATF6α functions as a UPR sensor/transducer but is a somewhat unfolded protein that is constitutively subjected to gpERAD (Haze et al., 1999; Horimoto et al., 2013). Degradation of ATF6α was blocked almost completely in SEL1L-KO and EDEM-TKO HCT116 cells (Fig. 1B), as was seen previously (Horimoto et al., 2013; Ninagawa et al., 2014); note that construction and characterization of SEL1L-KO cells were described in Figure 1-figure supplement 3. Strikingly, degradation of ATF6α was markedly accelerated in UGGT1-KO and UGGT-DKO cells but not in UGGT2-KO cells (Fig. 1C). These findings revealed for the first time that UGGTs are involved in not only folding but also ERAD. The fact that ATF6α was stabilized in UGGT-DKO cells treated with a mannosidase inhibitor, kifunensine, as in WT cells treated with kifunensine (Fig. 1D), showed that the acceleration of ATF6α degradation required mannose trimming.

We then examined the effect of DNJ, an inhibitor of glucosidase I and II (Fig. 1A). Stabilization of ATF6α in SEL1L-KO and EDEM-TKO cells was not affected by treatment with DNJ (Fig. 1B). This is because SEL1L is required for retrotranslocation (Fig. 1A), and because gpERAD requiring mannose trimming cannot work in EDEM-TKO cells, resulting in marked accumulation of M9 (Figure 1-figure supplement 4A); note that both retrotranslocation and mannose trimming are events downstream of glucose trimming (Fig 1A). The result obtained with EDEM-TKO cells indicates that ATF6α is still degraded via gpERAD requiring mannose trimming under the treatment with

glucosidase inhibitor.

In contrast, degradation of ATF6α in WT cells was slightly delayed by treatment with DNJ, and accelerated degradation of ATF6α in UGGT-DKO cells was compromised by treatment with DNJ, so that the degradation rate of ATF6α became very similar in WT or UGGT-DKO cells after treatment with DNJ (Fig. 1E). This implies the importance of glucose trimming-mediated production rate of M9 for efficient gpERAD. Indeed, the increase in the level of GM9 and the decrease in the level of M9 were observed in WT and UGGT-DKO cells treated with DNJ (Figure 1-figure supplement 4BC). Nonetheless, ATF6α was not stabilized completely in WT or UGGT-DKO cells treated with DNJ (Fig. 1E), unlike in EDEM-TKO and SEL1L-KO cells (Fig. 1B). We consider it likely that this is because mannose trimming still occurred in the absence of glucose trimming, as evidenced by the increased detection of GM8 in cells treated with DNJ (Figure 1-figure supplement 4BCD), leading to recognition of GM7 by OS9/XTP3B for retrotranslocation (Refer to Fig. 5). These results clearly showed that UGGT1 is actively involved in gpERAD of ATF6α; UGGT1-mediated reglucosylation reduces the probability of the mannose trimming that is prerequisite for gpERAD.

We next examined the effect of UGGT1/2 knockout on degradation of NHK, a soluble gpERAD substrate. NHK with three *N*-glycosylation sites is severely misfolded because of its C-terminus truncation resulting from TC deletion in the α1-antitrypsin (A1AT) gene (Sifers et al., 1988). We found that degradation of NHK was accelerated in UGGT1-KO and UGGT-DKO cells but not in UGGT2-KO cells (Fig. 2A), similar to the case of ATF6α. Of note, this acceleration required glucosyltransferase activity, as introduction of myc-tagged WT UGGT1 but not its catalytically inactive mutant, D1358A, into UGGT1-KO cells by transfection decelerated degradation of NHK (Fig. 2B). In

contrast, the degradation rate of NHK-QQQ, in which all three *N*-glycosylation sites in NHK were mutated (Ninagawa et al., 2015), was not affected by gene disruption of UGGT1 or UGGT2 (Fig. 2C).

We also found that degradation of CD3δ-ΔTM-HA, a soluble gpERAD substrate (Bernasconi et al., 2010), as well as degradation of its more severely misfolded form CD3δ-ΔTM-<33-7a-34>HA (Ninagawa et al., 2015) was accelerated in UGGT-DKO cells, albeit marginally (Fig. 2DE). Thus, UGGT-mediated reglucosylation affects the fate of unfolded, misfolded, and severely misfolded glycoproteins but not non-glycoproteins.

Effect of UGGT1/2 knockout on folded and functional proteins

We examined the effect of UGGT1/2 knockout on the stability of ER-localized endogenous proteins and found that they were stable both in WT and in UGGT-DKO cells no matter whether they were glycoproteins (Grp170, Sil1, and ribophorin I) or non-glycoproteins (CRT) (Fig. 3ABCD and Figure 3-figure supplement 1AB). Similarly, the activity of the Golgi-resident glycosyltransferase GnT-V (MGAT5) with six putative *N*-glycosylation sites (Hirata et al., 2023) was similar in WT, UGGT1-KO, UGGT2-KO and UGGT-DKO cells (Fig. 3E).

Interestingly, however, a truncated version of rat ribophorin I lacking its C-terminal region (aa333-606), termed rRI332-Flag, (Figure 3-figure supplement 1A) (de Virgilio et al., 1998; Mueller et al., 2006) was unstable in WT cells compared with ribophorin I when expressed by transfection, and its degradation rate was accelerated in UGGT1-KO and UGGT-DKO cells (Fig. 3D, right panel).

EMC1 is a type I membrane protein with three glycosylation sites, and is involved in insertion of membrane protein (Jonikas et al., 2009; Shurtleff et al., 2018). Endogenous EMC1 was a relatively stable protein in both WT and UGGT-DKO cells, but

when EMC1-ΔPQQ lacking the PQQ domain was transfected, the degradation rate of EMC1-ΔPQQ was accelerated in UGGT1-KO and UGGT-DKO cells (Fig. 3F), similarly to the case of ribophorin I vs rRI332-Flag. Thus, UGGT-mediated reglucosylation affects the fate of unstable proteins but not stable proteins.

UGGTs are required for the proper functioning of ATF6α

We finally investigated the physiological significance of preventing early degradation of substrates by UGGTs. Upon ER stress, a precursor form of ATF6α, designated ATF6α(P), is cleaved to the nucleus-localized form of ATF6α, designated ATF6α(N), to upregulate the ERSE and UPRE promoters, but not the ATF4 promoter (Mori, 2000; Yoshida et al., 1998). Degradation of ATF6α(P) was accelerated in UGGT1-deficient cells (Fig. 1), and accordingly the endogenous protein expression level of ATF6α(P) was decreased in UGGT1-deficient cells (Fig. 4A). Whereas degradation rate of ATF6α(P) was not changed in UGGT2-deficient cells, expression level of ATF6α(P) was decreased by a small amount (Fig. 4A p=0.06), suggesting that UGGT2 is also slightly involved in folding of ATF6α(P). The conversion from ATF6α(P) to ATF6α(N) is a marker for its activation. The amount of ATF6α(N) was decreased in UGGTs-KO at 1 hour after the treatment of thapsigargin (Tg), an inhibitor of the ER calcium pump (Fig. 4BCD). In addition, peak of activation was shifted from 1 hour to 4 hour after the treatment of Tg in UGGT1-KO cells. This can be explained by the rigid structure of ATF6α(P) lacking structural flexibility to respond to ER stress because the remaining ATF6α(P) in UGGT1-KO cells tends to have a more rigid structure that averts degradation, which is supported by its slightly weaker sensitivity to trypsin (Figure 4-figure supplement 1A). Then, we examined the effects of UGGTs on the activation level of ATF6α. In WT cells, the activity of ERSE and UPRE was upregulated 4.8 and 12.1-

fold by Tg, respectively, an effect that was abolished in ATF6α-KO cells. In UGGTs-KO cells, the level of induction of the ERSE and UPRE reporters decreased (Fig. 4EF), but the reporter activity of ATF4 upon Tg treatment did not decrease in UGGTs-KO cells (Fig. 4G). These results clearly show that UGGT1 and UGGT2 are required for proper functioning of ATF6α.

Our results show that UGGTs contribute significantly to the timing of substrate degradation. Previously, in higher animals, the activity of UGGTs was thought to contribute to glycoprotein folding and secretion but not to glycoprotein degradation, based on experiments using a glucosidase inhibitor (Tannous et al., 2015). The reason why the degradation rate was not changed significantly by DNJ can be explained by the activity of UGGTs and the efficiency of mannose trimming. In WT cells, UGGTs prevent early degradation by adding a glucose to facilitate further folding but mannose trimming occurs normally to promote degradation. In the presence of DNJ, the glycan-dependent folding pathway cannot work well to prevent early degradation, but mannose trimming does not occur at the normal rate due to a glucose residue on the A chain. Consequently, substrates in cells with DNJ treatment are degraded at approximately the same rate as ones in cells without DNJ. This is supported by our findings that there were no marked differences between WT and WT + DNJ, and UGGT-DKO + DNJ in the degradation of ATF6α (Fig. 1E and Fig. 5). In our experiments, we were able to evaluate the more direct effect of glucose reattachment by UGGTs on ERAD substrates and we found that UGGTs prevent early degradation of substrates.

This degradation-inhibitory effect of UGGTs, especially UGGT1, on early degradation was also observed for other model substrates in ERAD, such as NHK, CD3-δ-ΔTM, CD3-δ-ΔTM-<33-7aa-34>, EMC1-ΔPQQ and RI332, but not for native, stable

glycoproteins, such as Ribophorin I, EMC1, Grp170 and Sil1. Glycoproteins with stable conformational states do not require UGGTs, but to unstable, unassembled, conformationally abnormal and severely misfolded proteins, UGGTs give opportunities for proper folding by CNX/CRT, inhibiting their early degradation in the ER. Therefore, we conclude that the capability of reglucosylation has a huge impact on determining the timing of substrate degradation, and UGGTs usually act to prevent early degradation. Given the delayed substrate degradation in the KO of EDEMs (George et al., 2020; Leto et al., 2019; Ninagawa et al., 2015; Ninagawa et al., 2014), it is further concluded that UGGTs play a "tug-of-war" with EDEMs regarding the fate of glycoproteins: whether to give them a chance to fold, or to degrade them (Fig. 5).

How many glycoproteins undergo glucose re-addition by UGGTs and how many times those glycoproteins have experienced the CNX/CRT cycle is a subject for future work. Our findings strongly suggest that UGGTs are not just a CNX/CRT safety net, but should be a central component in the *N*-glycan-dependent folding pathway competing with the EDEMs-mediated degradation pathway.

MATERIALS AND METHODS

Statistics

Statistical analysis was conducted using Student's t-test, with probability expressed as *$p<0.05$ and **$p<0.01$ for all figures.

Construction of plasmids

Recombinant DNA techniques were performed using standard procedures (Sambrook et al., 1989) and the integrity of all constructed plasmids was confirmed by extensive sequencing analyses. Using 3xMyc-Fw and 3xMyc-Rv primers, Myc3 fragment was obtained from ATF6α(C)-TAP2 (Myc3-TEV-ProteinA) (George et al., 2021) and inserted into A p3xFlag-CMV-14 expression vector (Sigma) at the site of BamHI to construct p3xMyc-CMV-14 expression vector. Full-length open reading frame of human UGGT1 or UGGT2 was amplified using PrimeSTAR HS DNA polymerase and a pair of primers, namely, UGGT1-cloningFw and UGGT1-cloningRv for UGGT1, and UGGT2-cloningFw and UGGT2-cloningRv for UGGT2, respectively, from a cDNA library of HCT116 which was prepared using Moloney murine leukemia virus reverse transcriptase (Invitrogen), as described previously (Ninagawa et al., 2014). Site-directed mutagenesis was carried out with DpnI to construct UGGT1-D1358A-Myc3 using UGGT1-D1358AFw and UGGT1-D1358Arv primers and DpnI. Partial open reading frame of Rat Ribophorin I was amplified using a pair of primers, namely, RatRI332-cloningFw and RatRI332-cloningRv, and inserted into p3xFlag-CMV-14 or p3xMyc-CMV-14 between the HindIII and KpnI sites to construct RI332-Flag or RI332-Myc, respectively. Expression vectors of NHK, CD3-δ-ΔTM-HA, CD3-δ-ΔTM-<33-7aa-34>-HA, EMC1-ΔPQQ-Flag, A1AT and Hemagglutinin were described previously (Ninagawa et al., 2015; Ninagawa et al., 2014; Ninagawa et al., 2020b).

Cell culture and transfection

HCT116 cells (ATCC CCL-247) and HeLa cells (ATCC CCL-2) were cultured in Dulbecco's modified Eagle's medium (glucose 4.5 g/liter) supplemented with 10% fetal bovine serum, 2 mM glutamine, and antibiotics (100 U/ml penicillin and 100 mg/ml streptomycin) at 37°C in a humidified 5% CO_2/95% air atmosphere. Transfection was performed using polyethylenimine max (Polyscience) according to the manufacturer's instructions. EndoH was obtained from Calbiochem; cycloheximide from Sigma; MG132 from Peptide Institute; and Z-vad-fmk from Promega. No mycoplasma contamination confirmed by MycoBlue Mycoplasma Detector (Vazyme).

Immunological techniques

Immunoblotting analysis was carried out according to the standard procedure (Sambrook et al., 1989) as described previously (Ninagawa et al., 2011). Chemiluminescence obtained using Western Blotting Luminol Reagent (Santa Cruz Biotechnology) was detected using an LAS-3000mini Lumino-Image analyzer (Fuji Film). The antibodies used are listed in Supplemental material. Anti-human ATF6α (Haze et al., 1999) and EMC1 (Ninagawa et al., 2015) antibodies were produced previously. Immunoprecipitation was performed using the described antibodies and protein G- or A-coupled Sepharose beads (GE Healthcare). Beads were washed with high salt buffer (50 mM Tris/Cl, pH 8.0, containing 1% NP-40 and 150 mM NaCl) twice, washed with PBS, and boiled in Laemmli's sample buffer.

***N*-glycan profiling**

Pyridylamination and structural identification of *N*-glycans of total cellular glycoproteins were performed as described previously (Horimoto et al., 2013; Ninagawa et al., 2014).

Pulse-chase experiments

Pulse-chase experiments using 9.8 Mbq per dish of EASY-TAG EXPRESS Protein labeling mix [^{35}S] (PerkinElmer) and subsequent immunoprecipitation using suitable antibodies and protein G or A-coupled Sepharose beads (GE Healthcare) were performed according to our published procedure (Ninagawa et al., 2014).

CRISPR/Cas9 method to generate KO cell lines of UGGT1

Using the pair of primers UGGT1sgRNAFw and Rv, the sequences of the BbsI site of px330 (Addgene) was converted to that to express sgRNA for cleavage at exon 2 of the UGGT1 gene. PuroR and backbone fragment were amplified by PCR from DT-A-pA-loxP-PGK-Puro-pA-loxP (Ninagawa et al., 2014) using UGGT1-PuroFw and Rv primers, and UGGT1-BackboneFw and UGGT1-BackboneRv primers, respectively. Left and right arms were amplified by PCR from the human genome originated from HCT116 using UGGT1-LarmFw and Rv, and UGGT1-RarmFw and Rv. Four fragments were built up using an NEBuilder HiFi DNA Assembly Cloning Kit (New England Biolabs) to create pKO-hUGGT1-Puro, which was transfected into HCT116 cells with sgRNA expression vector for UGGT1. Clones with puromycin (0.5 μg/ml) resistance were selected.

CRISPR/Cas9 method to generate KO cell lines of UGGT2

Using the pair of primers UGGT2sgRNAFw and Rv, the sequence of the BbsI site of px330 (Addgene) was converted to that to express sgRNA for cleavage at exon 4 of the UGGT2 gene. Hygro^{r} and backbone fragment were amplified by PCR from DT-A-pA-loxP-PGK-Hygro-pA-loxP (Tsuda et al., 2019) using UGGT2-HygroFw and Rv primers, and UGGT2-BackboneFw and UGGT2-BackboneRv primers, respectively. Left and right arms were amplified by PCR from human genome originated from HCT116 using UGGT2-LarmFw and Rv primers, and UGGT2-RarmFw and Rv primers, respectively. Four fragments were built up using an NEBuilder HiFi DNA Assembly Cloning Kit to

create pKO-hUGGT2-Hygro, which was transfected into HCT116 cells with sgRNA expression vector for UGGT2. Clones with hygromycin (300 μg/ml) resistance were selected.

TALEN method to generate KO cell lines of SEL1L

Platinum TALEN plasmid was constructed as described previously (Ninagawa et al., 2014; Sakuma et al., 2013). In brief, each DNA-binding module was assembled into ptCMV-153/47-VR vectors using the two-step Golden Gate cloning method. The assembled sequence was 5-TGCTGCTGTGTGCGGTGCTgctgagcttggccTCGGCGTCCTCGGGTCA-3, where uppercase and lowercase letters indicate TALEN target sequences and spacer sequences, respectively.

Reporter assay

Twenty-four hours after transfection, HCT116 cells cultured in a 24-well plate were washed with PBS and lysed in Luciferase Assay Lysis Buffer (Toyo Bnet). Luciferase activity was determined using PicaGene Dual-luciferase reporter assay reagent (Toyo Bnet). Relative luciferase activity was defined as the ratio of firefly luciferase activity to renilla luciferase activity. ERSE, UPRE and ATF4 reporters were described previously (Saito et al., 2022). Briefly, the ERSE reporter is pGL3-GRP78(-132)-Luc carrying the human BiP promoter, the UPRE reporter carries p5xUPRE-GL3 identical to p5xATF6GL3, and the ATF4 reporter carries the promoter region of murine ATF4 from position –261 to +124 (ORF starts at +1).

Measurement of glycosyltransferase activities

The experiment was described previously (Hirata et al., 2023). Briefly, 3 μl of the cell lysates was incubated in a total of 10 μl of a reaction buffer [125 mM MES (pH 6.25), 10

mM $MnCl_2$, 200 mM GlcNAc, 0.5% Triton X-100, and 1 mg/ml BSA] supplemented with 20 mM UDP-GlcNAc and 10 μM fluorescence-labeled biantennary acceptor *N*-glycan substrate GnGnbi-PA (PA, 2-aminopyridine) at 37 ℃ for 3 h. After the reaction, the sample was boiled at 99 ℃ for 2 min to inactivate the enzymes and then 40 μl of water was added. After centrifugation at 21,500 *g* for 5 min, the supernatants were analyzed by reverse-phase HPLC with an ODS column (4.6 x 150 mm, TSKgel ODS-80TM; TOSOH Bioscience). HPLC analysis was conducted in the isocratic mode in which 80% buffer A (20 mM ammonium acetic buffer (pH 4.0)) and 20% buffer B (1% butanol in buffer A) were loaded at 1 ml/min.

Trypsin digestion assay

The trypsin digestion assay was described previously (Ninagawa and Mori, 2016; Ninagawa et al., 2015).

ACKNOWLEDGEMENTS

The authors declare no competing financial interests. We are grateful to the members of Biosignal Research Center, Graduate School of Agriculture, Kobe University, and Graduate School of Science, Kyoto University for helpful discussions and encouragement. We appreciate the kind cooperation of the Research Facility Center for Science and Technology, Kobe University. We thank Ms. Shino Oguri, Ms. Kaoru Miyagawa, Ms. Makiko Sawada and Ms. Yuko Tokoro for their technical and secretarial assistance, and Dr. Masayuki Yokoi (Kobe University) for his help in the use of GloMax. This work was financially supported in part by the Ministry of Education, Culture, Sports, Science and Technology, MEXT, Japan (18K06216 to S.N., 21H02625 and 23H03838 to H.Y., and 17H01432, 17H06419 and 22H00407 to K.M.), the Takeda Science Foundation (to S. N.), the Kobayashi Foundation (to S. N.), the Naito Foundation, and Nagase Science & Technology Foundation (to S. N.) and a donation from Dr. Takahiko Nagamine of Sunlight Brain Research Center (to S. N.). This work was supported by Joint Research of the Exploratory Research Center on Life and Living Systems (ExCELLS) (ExCELLS program No, 21-307) and the Assisted Joint Research Program (Exploration Type) of the J-GlycoNet cooperative network (Support-18), which is accredited by MEXT, Japan, as a Joint Usage/Research Center.

REFERENCES

Adams, B.M., N.P. Canniff, K.P. Guay, I.S.B. Larsen, and D.N. Hebert. 2020. Quantitative glycoproteomics reveals cellular substrate selectivity of the ER protein quality control sensors UGGT1 and UGGT2. *Elife*. 9.

Bernasconi, R., C. Galli, V. Calanca, T. Nakajima, and M. Molinari. 2010. Stringent requirement for HRD1, SEL1L, and OS-9/XTP3-B for disposal of ERAD-LS substrates. *J Cell Biol*. 188:223-235.

Berner, N., K.R. Reutter, and D.H. Wolf. 2018. Protein Quality Control of the Endoplasmic Reticulum and Ubiquitin-Proteasome-Triggered Degradation of Aberrant Proteins: Yeast Pioneers the Path. *Annual review of biochemistry*. 87:751-782.

Brodsky, J.L., and W.R. Skach. 2011. Protein folding and quality control in the endoplasmic reticulum: Recent lessons from yeast and mammalian cell systems. *Curr Opin Cell Biol*. 23:464-475.

Caramelo, J.J., O.A. Castro, G. de Prat-Gay, and A.J. Parodi. 2004. The endoplasmic reticulum glucosyltransferase recognizes nearly native glycoprotein folding intermediates. *J Biol Chem*. 279:46280-46285.

de Virgilio, M., H. Weninger, and N.E. Ivessa. 1998. Ubiquitination is required for the retro-translocation of a short-lived luminal endoplasmic reticulum glycoprotein to the cytosol for degradation by the proteasome. *J Biol Chem*. 273:9734-9743.

Ferris, S.P., N.S. Jaber, M. Molinari, P. Arvan, and R.J. Kaufman. 2013. UDP-glucose:glycoprotein glucosyltransferase (UGGT1) promotes substrate solubility in the endoplasmic reticulum. *Molecular biology of the cell*. 24:2597-2608.

George, G., S. Ninagawa, H. Yagi, J.I. Furukawa, N. Hashii, A. Ishii-Watabe, Y. Deng, K. Matsushita, T. Ishikawa, Y.P. Mamahit, Y. Maki, Y. Kajihara, K. Kato, T. Okada, and K. Mori. 2021. Purified EDEM3 or EDEM1 alone produces determinant oligosaccharide structures from M8B in mammalian glycoprotein ERAD. *Elife*. 10.

George, G., S. Ninagawa, H. Yagi, T. Saito, T. Ishikawa, T. Sakuma, T. Yamamoto, K. Imami, Y. Ishihama, K. Kato, T. Okada, and K. Mori. 2020. EDEM2 stably disulfide-bonded to TXNDC11 catalyzes the first mannose trimming step in mammalian glycoprotein ERAD. *Elife*. 9:e53455.

Haze, K., H. Yoshida, H. Yanagi, T. Yura, and K. Mori. 1999. Mammalian transcription factor ATF6 is synthesized as a transmembrane protein and activated by proteolysis in response to endoplasmic reticulum stress. *Molecular biology of the*

cell. 10:3787-3799.

Helenius, A., and M. Aebi. 2004. Roles of N-linked glycans in the endoplasmic reticulum. *Annual review of biochemistry*. 73:1019-1049.

Hirao, K., Y. Natsuka, T. Tamura, I. Wada, D. Morito, S. Natsuka, P. Romero, B. Sleno, L.O. Tremblay, A. Herscovics, K. Nagata, and N. Hosokawa. 2006. EDEM3, a soluble EDEM homolog, enhances glycoprotein endoplasmic reticulum-associated degradation and mannose trimming. *J Biol Chem*. 281:9650-9658.

Hirata, T., Y. Harada, K.M. Hirosawa, Y. Tokoro, K.G.N. Suzuki, and Y. Kizuka. 2023. N-acetylglucosaminyltransferase-V (GnT-V)-enriched small extracellular vesicles mediate N-glycan remodeling in recipient cells. *iScience*. 26:105747.

Horimoto, S., S. Ninagawa, T. Okada, H. Koba, T. Sugimoto, Y. Kamiya, K. Kato, S. Takeda, and K. Mori. 2013. The unfolded protein response transducer ATF6 represents a novel transmembrane-type endoplasmic reticulum-associated degradation substrate requiring both mannose trimming and SEL1L protein. *J Biol Chem*. 288:31517-31527.

Hung, H.H., Y. Nagatsuka, T. Solda, V.K. Kodali, K. Iwabuchi, H. Kamiguchi, K. Kano, I. Matsuo, K. Ikeda, R.J. Kaufman, M. Molinari, P. Greimel, and Y. Hirabayashi. 2022. Selective involvement of UGGT variant: UGGT2 in protecting mouse embryonic fibroblasts from saturated lipid-induced ER stress. *Proc Natl Acad Sci U S A*. 119:e2214957119.

Ito, Y., Y. Kajihara, and Y. Takeda. 2020. Chemical-Synthesis-Based Approach to Glycoprotein Functions in the Endoplasmic Reticulum. *Chemistry*. 26:15461-15470.

Itzhak, D.N., S. Tyanova, J. Cox, and G.H. Borner. 2016. Global, quantitative and dynamic mapping of protein subcellular localization. *Elife*. 5.

Jonikas, M.C., S.R. Collins, V. Denic, E. Oh, E.M. Quan, V. Schmid, J. Weibezahn, B. Schwappach, P. Walter, J.S. Weissman, and M. Schuldiner. 2009. Comprehensive characterization of genes required for protein folding in the endoplasmic reticulum. *Science (New York, N.Y.)*. 323:1693-1697.

Lamriben, L., J.B. Graham, B.M. Adams, and D.N. Hebert. 2016. N-Glycan-based ER Molecular Chaperone and Protein Quality Control System: The Calnexin Binding Cycle. *Traffic*. 17:308-326.

Leto, D.E., D.W. Morgens, L. Zhang, C.P. Walczak, J.E. Elias, M.C. Bassik, and R.R. Kopito. 2019. Genome-wide CRISPR Analysis Identifies Substrate-Specific Conjugation Modules in ER-Associated Degradation. *Mol Cell*. 73:377-389 e311.

Mori, K. 2000. Tripartite management of unfolded proteins in the endoplasmic reticulum.

Cell. 101:451-454.

Mueller, B., B.N. Lilley, and H.L. Ploegh. 2006. SEL1L, the homologue of yeast Hrd3p, is involved in protein dislocation from the mammalian ER. *J Cell Biol*. 175:261-270.

Ninagawa, S., G. George, and K. Mori. 2020a. Mechanisms of productive folding and endoplasmic reticulum-associated degradation of glycoproteins and non-glycoproteins. *Biochim Biophys Acta Gen Subj*:129812.

Ninagawa, S., and K. Mori. 2016. Trypsin Sensitivity Assay to Study the Folding Status of Proteins. *Bio-Protocol*. 6:e1953.

Ninagawa, S., T. Okada, Y. Sumitomo, S. Horimoto, T. Sugimoto, T. Ishikawa, S. Takeda, T. Yamamoto, T. Suzuki, Y. Kamiya, K. Kato, and K. Mori. 2015. Forcible destruction of severely misfolded mammalian glycoproteins by the non-glycoprotein ERAD pathway. *J Cell Biol*. 211:775-784.

Ninagawa, S., T. Okada, Y. Sumitomo, Y. Kamiya, K. Kato, S. Horimoto, T. Ishikawa, S. Takeda, T. Sakuma, T. Yamamoto, and K. Mori. 2014. EDEM2 initiates mammalian glycoprotein ERAD by catalyzing the first mannose trimming step. *J Cell Biol*. 206:347-356.

Ninagawa, S., T. Okada, S. Takeda, and K. Mori. 2011. SEL1L is required for endoplasmic reticulum-associated degradation of misfolded luminal proteins but not transmembrane proteins in chicken DT40 cell line. *Cell Struct Funct*. 36:187-195.

Ninagawa, S., S. Tada, M. Okumura, K. Inoguchi, M. Kinoshita, S. Kanemura, K. Imami, H. Umezawa, T. Ishikawa, R.B. Mackin, S. Torii, Y. Ishihama, K. Inaba, T. Anazawa, T. Nagamine, and K. Mori. 2020b. Antipsychotic olanzapine-induced misfolding of proinsulin in the endoplasmic reticulum accounts for atypical development of diabetes. *eLife*. 9:e60970.

Pearse, B.R., T. Tamura, J.C. Sunryd, G.A. Grabowski, R.J. Kaufman, and D.N. Hebert. 2010. The role of UDP-Glc:glycoprotein glucosyltransferase 1 in the maturation of an obligate substrate prosaposin. *J Cell Biol*. 189:829-841.

Saito, S., T. Ishikawa, S. Ninagawa, T. Okada, and K. Mori. 2022. A motor neuron disease-associated mutation produces non-glycosylated Seipin that induces ER stress and apoptosis by inactivating SERCA2b. *Elife*. 11.

Sakuma, T., H. Ochiai, T. Kaneko, T. Mashimo, D. Tokumasu, Y. Sakane, K. Suzuki, T. Miyamoto, N. Sakamoto, S. Matsuura, and T. Yamamoto. 2013. Repeating pattern of non-RVD variations in DNA-binding modules enhances TALEN activity. *Sci Rep*. 3:3379.

Sambrook, J., E.F. Fritsch, and T. Maniatis. 1989. Molecular cloning: a laboratory manual. Cold spring harbor laboratory press.

Shurtleff, M.J., D.N. Itzhak, J.A. Hussmann, N.T. Schirle Oakdale, E.A. Costa, M. Jonikas, J. Weibezahn, K.D. Popova, C.H. Jan, P. Sinitcyn, S.S. Vembar, H. Hernandez, J. Cox, A.L. Burlingame, J.L. Brodsky, A. Frost, G.H. Borner, and J.S. Weissman. 2018. The ER membrane protein complex interacts cotranslationally to enable biogenesis of multipass membrane proteins. *Elife*. 7.

Sifers, R.N., S. Brashears-Macatee, V.J. Kidd, H. Muensch, and S.L. Woo. 1988. A frameshift mutation results in a truncated alpha 1-antitrypsin that is retained within the rough endoplasmic reticulum. *J Biol Chem*. 263:7330-7335.

Smith, M.H., H.L. Ploegh, and J.S. Weissman. 2011. Road to ruin: targeting proteins for degradation in the endoplasmic reticulum. *Science (New York, N.Y.)*. 334:1086-1090.

Sousa, M., and A.J. Parodi. 1995. The molecular basis for the recognition of misfolded glycoproteins by the UDP-Glc:glycoprotein glucosyltransferase. *EMBO J*. 14:4196-4203.

Sousa, M.C., M.A. Ferrero-Garcia, and A.J. Parodi. 1992. Recognition of the oligosaccharide and protein moieties of glycoproteins by the UDP-Glc:glycoprotein glucosyltransferase. *Biochemistry*. 31:97-105.

Sun, Z., and J.L. Brodsky. 2019. Protein quality control in the secretory pathway. *J Cell Biol*. 218:3171-3187.

Takeda, Y., A. Seko, M. Hachisu, S. Daikoku, M. Izumi, A. Koizumi, K. Fujikawa, Y. Kajihara, and Y. Ito. 2014. Both isoforms of human UDP-glucose:glycoprotein glucosyltransferase are enzymatically active. *Glycobiology*. 24:344-350.

Tannous, A., N. Patel, T. Tamura, and D.N. Hebert. 2015. Reglucosylation by UDP-glucose:glycoprotein glucosyltransferase 1 delays glycoprotein secretion but not degradation. *Molecular biology of the cell*. 26:390-405.

Tessier, D.C., D. Dignard, A. Zapun, A. Radominska-Pandya, A.J. Parodi, J.J. Bergeron, and D.Y. Thomas. 2000. Cloning and characterization of mammalian UDP-glucose glycoprotein: glucosyltransferase and the development of a specific substrate for this enzyme. *Glycobiology*. 10:403-412.

Tsuda, M., S. Ogawa, M. Ooka, K. Kobayashi, K. Hirota, M. Wakasugi, T. Matsunaga, T. Sakuma, T. Yamamoto, S. Chikuma, H. Sasanuma, M. Debatisse, A.J. Doherty, R.P. Fuchs, and S. Takeda. 2019. PDIP38/PolDIP2 controls the DNA damage tolerance pathways by increasing the relative usage of translesion DNA synthesis over template switching. *PLoS One*. 14:e0213383.

van der Goot, A.T., M.M.P. Pearce, D.E. Leto, T.A. Shaler, and R.R. Kopito. 2018. Redundant and Antagonistic Roles of XTP3B and OS9 in Decoding Glycan and Non-glycan Degrons in ER-Associated Degradation. *Mol Cell*. 70:516-530 e516.

Yoshida, H., K. Haze, H. Yanagi, T. Yura, and K. Mori. 1998. Identification of the cis-acting endoplasmic reticulum stress response element responsible for transcriptional induction of mammalian glucose-regulated proteins. Involvement of basic leucine zipper transcription factors. *J Biol Chem*. 273:33741-33749.

LEGENDS TO FIGURES

Fig. 1 Effect of UGGT1/2-KO on degradation of ATF6α

(A) Schematic presentation of *N*-glycan processing and gpERAD.

(B) Cycloheximide chase (50 μg/ml) to determine degradation rate of endogenous ATF6α in WT, EDEM-TKO and SEL1L-KO cells treated with or without 0.5 mM DNJ treatment. DNJ was added 2 hours before the addition of CHX. Endogenous ATF6α was detected by immunoblotting using anti-ATF6α antibody. The means from three independent experiments with standard deviations (error bars) are plotted against the chase period (n = 3). P value: *<0.05, **<0.01.

(C) Cycloheximide chase (50 μg/ml) to determine degradation rate of endogenous ATF6α in WT, UGGT1-KO, UGGT2-KO and UGGT-DKO cells (n=3) as in (B). # denotes a non-specific band. P value: *<0.05, **<0.01.

(D) Cycloheximide chase (50 μg/ml) to determine degradation rate of endogenous ATF6α in WT and UGGT-DKO cells with or without 10 μg/ml kifunensine (Kif) treatment (n=3), as in (B). Kifunensine was added 1 hour before the addition of CHX. P value: *<0.05, **<0.01.

(E) Cycloheximide chase (50 μg/ml) to determine degradation rate of endogenous ATF6α in WT and UGGT-DKO treated with or without 0.5 mM DNJ (n = 3), as in (B). DNJ was added 2 hours before the addition of CHX. P value: *<0.05, **<0.01.

Fig. 2 Effect of UGGT1/2-KO on degradation of soluble ERAD substrates

(A) Pulse-chase and subsequent immunoprecipitation experiments using anti-α1-PI antibody to determine degradation rate of NHK in WT, UGGT1-KO, UGGT2-KO and UGGT-DKO cells transfected with plasmid to express NHK (n=3). The

radioactivity of each band was determined and normalized with the value at chase period 0 h. The means from three independent experiments with standard deviations (error bars) are plotted against the chase period (n = 3). P value: *<0.05, **<0.01.

(B) Rescue experiments using WT and UGGT1-KO cells transfected with plasmid to express NHK together with or without plasmid to express Myc-UGGT1 or Myc-UGGT1-D1358A (n = 3), as in (A). P value: *<0.05, **<0.01.

(C) Pulse-chase and subsequent immunoprecipitation experiments to determine degradation rate of NHK-QQQ in WT, UGGT1-KO and UGGT2-KO cells transfected with plasmid to express NHK-QQQ using anti-α1-PI antibody (n=3), as in (A).

(D) Pulse-chase and subsequent immunoprecipitation experiments using anti-HA antibody to determine degradation rate of CD3-δ-ΔTM-HA in WT, UGGT1-KO, UGGT2-KO and UGGT-DKO cells transfected with plasmid to express CD3-δ-ΔTM-HA (n =3), as in (A). P value: *<0.05.

(E) Pulse-chase and subsequent immunoprecipitation experiments using anti-HA antibody to determine the degradation rate of CD3-δ-ΔTM-<33-7aa-34>-HA in WT, UGGT1-KO, UGGT2-KO and UGGT-DKO cells transfected with plasmid to express CD3-δ-ΔTM-<33-7aa-34>-HA (n =3), as in (A). P value: *<0.05, **<0.01.

Fig. 3 Effect of UGGT1/2-KO on functional proteins in the secretory pathway and on their unstable mutants

(A)–(C) Cycloheximide chase (50 μg/ml) and subsequent immunoblotting experiments to determine the degradation rate of endogenous Grp170 (A), Sil1 (B) and CRT (C) in WT and UGGT-DKO cells using the respective antibody (n = 3).

(D) [left] Cycloheximide chase (50 μg/ml) and subsequent immunoblotting experiments

to determine the degradation rate of endogenous Ribophorin I in WT and UGGT-DKO cells using anti-Ribophorin antibody (n=3), as in (A). [right] Pulse chase and subsequent immunoprecipitation experiments using anti-Flag antibody to determine the degradation rate of rRI332-Flag in WT, UGGT1-KO, UGGT2-KO and UGGT-DKO cells transfected with plasmid to express rRI332-Flag (n =3), as in Fig. 3A. P value: *<0.05, **<0.01.

(E) Determination of GnT-V activity in cell lysate of WT, UGGT1-KO, UGGT2-KO and UGGT-DKO cells (n=3).

(F) Pulse-chase and subsequent immunoprecipitation experiments using anti-EMC1 antibody to determine degradation rate of endogenous EMC1 and EMC1-ΔPQQ-Flag in WT, UGGT1-KO, UGGT2-KO and UGGT-DKO cells transfected with plasmid to express EMC1-ΔPQQ-Flag (n =3), as in Fig. 3A. P value: *<0.05, **<0.01.

Fig. 4 Effects of UGGTs on unfolded protein response via ATF6α

(A) Immunoblotting to determine the protein level of ATF6α(P) in WT, UGGT1-KO, UGGT2-KO, UGGT-DKO, ATF6α-KO cells using anti-ATF6α antibody (n=3). P value: *<0.05.

(B–D) HCT116 cells cultured in 35-mm dishes were incubated in the presence of 300 nM thapsigargin (Tg) for the indicated periods. Endogenous ATF6α(P) and ATF6α(N) in WT was detected together with UGGT1-KO (B), UGGT2-KO (C), and UGGT-DKO (D), respectively. # indicates non-specific band.

(E-G) HCT116 cells transiently transfected with ERSE (E), UPRE (F) or ATF4 (G) reporters. Twenty-four hours after the transfection, cells were treated with 300 nM Tg for 6 h and harvested to determine luciferase activity (n=3). Relative activity of Luciferase

and Renilla, and fold induction of Tg + and Tg – are shown.

Figure 5 Model of behavior of glycoproteins in the ER

(A). In WT cells, glycoproteins with M9 or M8 are recognized by UGGTs to produce GM9 or GM8 to promote their folding by CNX or CRT, or by EDEMs to trim mannoses of *N*-glycan to expose the α1,6-bond of *N*-glycan in the C chain for gpERAD. Glycoproteins are caught in a tug-of-war between the fate of structure formation by UGGTs and degradation by EDEMs. (B). In WT cells with DNJ, glycoproteins are degraded by EDEMs-mediated gpERAD despite inefficiency of mannose trimming due to the presence of glucoses at A chain. (C). In UGGT-DKO cells, glycoproteins are subjected to premature degradation by EDEMs-mediated gpERAD. (D). In UGGT-DKO cells with DNJ, the almost the same situation as in (B) exists. (E–F). In EDEM-TKO cells, glycoproteins are not degraded via gpERAD.

Figure 1-Figure supplement 1 Generation of UGGT1/2-KO HCT116 cells

(A) Strategy for obtaining UGGT1-KO, UGGT2-KO and UGGT-DKO cells from HCT116 cells. UGGT1-KO #2, UGGT2-KO #2 and UGGT-DKO #2 were mainly used in this report.

(B) Schematic presentation of UGGT1 and UGGT2 loci.

(C) Strategy of the CRISPR/Cas9-mediated targeting of exon 2 of the UGGT1 gene.

(D) Strategy of the CRISPR/Cas9-mediated targeting of exon 4 of the UGGT2 gene.

(E) Genomic PCR to confirm recombination of UGGT1 locus.

(F) Genomic PCR to confirm recombination of UGGT2 locus.

(G) RT-PCR to amplify cDNA corresponding to full length UGGT1 from WT and two

independent UGGT1-KO cell lines (#1 and #2).

(H) RT-PCR to amplify cDNA corresponding to full length UGGT2 from WT and two independent UGGT2-KO cell lines (#1 and #2).

(I) Schematic presentation of UGGT1 mRNA expressed in two independent UGGT1-KO cell lines (#1 and #2) and their translational products. The sequence of the amplified cDNA in (G) was determined.

(J) Schematic presentation of UGGT2 mRNA expressed from the deleted and targeted alleles in UGGT2-KO cell lines and their translational products. The sequence of the amplified cDNA in (H) was determined

(K) Immunoblotting to determine endogenous protein expression of UGGT1 and UGGT2 in UGGT1-KO, UGGT2-KO and UGGT-DKO HCT116 cells using anti-UGGT1, anti-UGGT2 and anti-GAPDH antibodies.

(L) Doubling time of WT, UGGT1-KO, UGGT2-KO and UGGT-DKO HCT116 cells (n = 3).

Figure 1-Figure supplement 2 Generation and characterization of UGGT1/2-KO HCT116 cells

(A) Immunoblotting of cell lysates prepared from WT HCT116 and HeLa cells transiently expressing UGGT1-Myc3 or UGGT2-Myc3 using anti-Myc, anti-UGGT1, anti-UGGT2 and anti-GAPDH antibodies. The intensity of the lower left band in each panel is set to 1.00, and relative intensities are shown below. Anti-Myc antibody was used to estimate the ratio of the amounts of UGGT1-Myc3 and UGGT2-Myc3. Anti-UGGT1 antibody was used to estimate that of endogenous UGGT1 and UGGT1-Myc3. Anti-UGGT2 antibody was used to estimate that of endogenous UGGT2 and UGGT2-Myc3. These values can

be used to calculate the relative amounts of endogenous UGGT1 and UGGT2. Approximate expression level of UGGT2 relative to UGGT1 in HCT116 and HeLa cells shown as % in bottom panel.

(B) Expression levels of BiP, XBP1(S), spliced form of XBP1, ATF4 and GAPDH determined by immunoblotting of cell lysates, which were prepared from WT, WT treated with 300 nM thapsigargin (Tg) for 6 h, UGGT1-KO, UGGT2-KO and UGGT-DKO cells.

(C) Schematic presentation of UGGT1 and UGGT2 proteins with potential *N*-glycosylation sites and catalytic domain indicated. Cell lysates were prepared from WT HCT116 cells, treated or not treated with EndoH, and analyzed by immunoblotting using anti-UGGT1 and anti-UGGT2 antibodies.

(D), (E) Secretion of A1AT (D) and EPO-Myc3 (E) in WT, UGGT1-KO, UGGT2-KO and UGGT-DKO HCT116 cells. Cells were transfected with plasmid to express A1AT or EPO-Myc3. Twenty-four hours later, cells were pulse labeled with ^{35}S-methionine and cysteine for 20 min and then chased for the indicated periods, followed by immunoprecipitation of A1AT or EPO-Myc3 from cells and medium using anti-A1AT or anti-Myc antibody, respectively, and then subjected to reducing SDS-PAGE and autoradiography (n=3). The amount of A1AT or EPO-Myc3 in WT cells at 0 min was set as 100 %. The means from three independent experiments with standard deviations (error bars) were plotted against the chase period.

(F) Maturation of HA in WT, UGGT1-KO, UGGT2-KO and UGGT-DKO HCT116 cells. Pulse-chase experiments were conducted using various cells transfected with plasmid to express HA, followed by immunoprecipitation of HA from cells using anti-HA antibody (n=3), as in (D). The immunoprecipitates were digested with EndoH prior to subjection to reducing SDS-PAGE. The amount of HA with high-mannose type *N*-glycan at time 0

h in WT cells was set as 100 %.

Figure 1-figure supplement 3 Generation of SEL1L-KO HCT116 cells

(A) Schematic presentation of SEL1L locus

(B) Strategy of the TALEN-mediated targeting of exon 1 of the SEL1L gene.

(C) Genomic PCR to confirm recombination of SEL1L locus.

(D) RT-PCR to amplify cDNA corresponding to full length SEL1L from WT and two independent SEL1L-KO cell lines (#1 and #2).

(E) Immunoblotting of SEL1L protein in WT and two independent SEL1L-KO cell lines (#1 and #2) using anti-SEL1L antibody.

(F) Doubling time of WT and two independent SEL1L-KO cell lines (#1 and #2).

Figure 1-Figure supplement 4 *N*-glycan profiling of various types of cells treated or not treated with DNJ

(A)–(D) Isomer composition of high mannose-type *N*-glycans prepared from total cellular glycoproteins of WT, UGGT-DKO and EDEM-TKO cells (A), WT cells treated with or without 0.5 mM DNJ for 16 h (B), UGGT-DKO cells treated with or without 0.5 mM DNJ for 16 h (C), EDEM-TKO cells treated with or without 0.5 mM DNJ for 16 h (D). This experiment was completed once.

Figure 3-Figure supplement 1 Characterization of various proteins present in the secretory pathway

(A) Schematic structures of human Grp170, human Sil1, human CRT, human GnT-V, human Ribophorin I, rat Ribophorin I, human EMC1, and human EMC1-ΔPQQ-Flag with

potential *N*-glycosylation sites indicated. It has not been confirmed whether two *N*-glycans are attached to human and rat Ribophorin I. Sequence identities between human and rat Ribophorin I are shown as percentages. rRI332-Flag lacks aa 333–606 of rat Ribophorin I.

(B) Immunoblotting with respective antibody of cells lysates prepared from WT cells and cells treated with or without EndoH treatment.

Figure 4-Figure supplement 1 Structural assessment of ATF6α in UGGT1-KO

(A) Trypsin digestion assay to evaluate the folding state of ATF6α(P) in WT and UGGT1-KO. The same amounts of proteins in cell lysate from WT and UGGT1-KO cells were treated with the indicated concentration of trypsin for 15 minutes at room temperature. Enzymatic activity of trypsin was terminated by addition of Laemmli SDS sample buffer containing 100 mM DTT and 10x protease inhibitor cocktail. Immunoblotting was conducted as in Fig. 4A, using anti-ATF6α and anti-Sil1 antibodies. In electrophoresis for the detection of ATF6α, the UGGT1-KO sample is loaded with twice as much protein as the WT sample.

Figure. 1

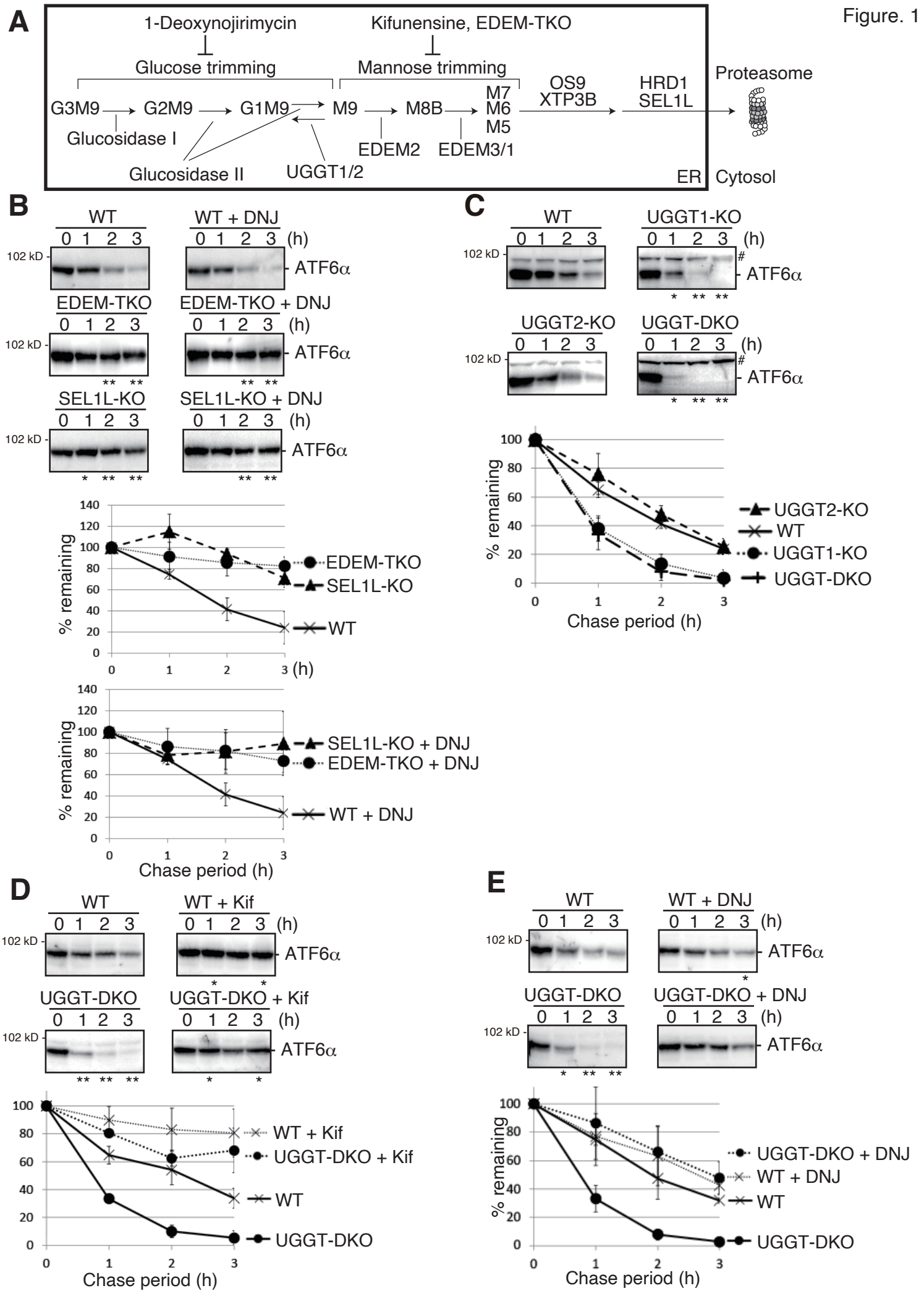
A
1-Deoxynojirimycin
Kifunensine, EDEM-TKO
Glucose trimming
Mannose trimming
G3M9
G2M9
G1M9
M9
M8B
M7
M6
M5
OS9
XTP3B
HRD1
SEL1L
Proteasome
Glucosidase I
Glucosidase II
UGGT1/2
EDEM2
EDEM3/1
ER
Cytosol
B
WT
WT + DNJ
EDEM-TKO
EDEM-TKO + DNJ
SEL1L-KO
SEL1L-KO + DNJ
102 kD
ATF6α
(h)
% remaining
Chase period (h)
EDEM-TKO
SEL1L-KO
WT
SEL1L-KO + DNJ
EDEM-TKO + DNJ
WT + DNJ
C
WT
UGGT1-KO
UGGT2-KO
UGGT-DKO
UGGT2-KO
WT
UGGT1-KO
UGGT-DKO
D
WT
WT + Kif
UGGT-DKO
UGGT-DKO + Kif
WT + Kif
UGGT-DKO + Kif
WT
UGGT-DKO
E
WT
WT + DNJ
UGGT-DKO
UGGT-DKO + DNJ
UGGT-DKO + DNJ
WT + DNJ
WT
UGGT-DKO

Figure. 2

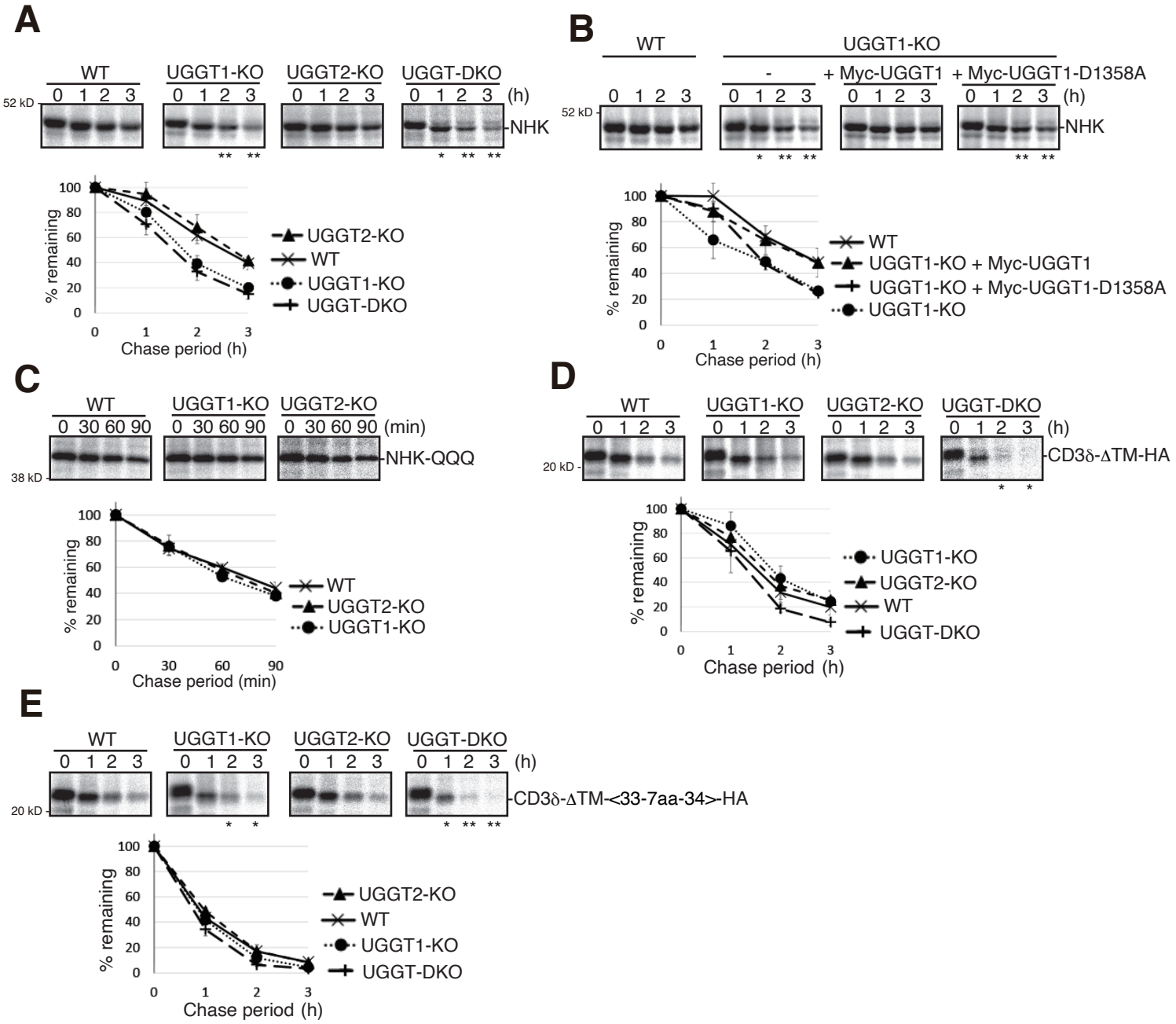
A
WT
UGGT1-KO
UGGT2-KO
UGGT-DKO
0 1 2 3
(h)
52 kD
NHK
% remaining
Chase period (h)
UGGT2-KO
WT
UGGT1-KO
UGGT-DKO
B
WT
UGGT1-KO
-
+ Myc-UGGT1
+ Myc-UGGT1-D1358A
52 kD
NHK
% remaining
Chase period (h)
WT
UGGT1-KO + Myc-UGGT1
UGGT1-KO + Myc-UGGT1-D1358A
UGGT1-KO
C
WT
UGGT1-KO
UGGT2-KO
0 30 60 90
(min)
38 kD
NHK-QQQ
% remaining
Chase period (min)
WT
UGGT2-KO
UGGT1-KO
D
WT
UGGT1-KO
UGGT2-KO
UGGT-DKO
0 1 2 3
(h)
20 kD
CD3δ-ΔTM-HA
% remaining
Chase period (h)
UGGT1-KO
UGGT2-KO
WT
UGGT-DKO
E
WT
UGGT1-KO
UGGT2-KO
UGGT-DKO
0 1 2 3
(h)
20 kD
CD3δ-ΔTM-<33-7aa-34>-HA
% remaining
Chase period (h)
UGGT2-KO
WT
UGGT1-KO
UGGT-DKO

Figure. 3

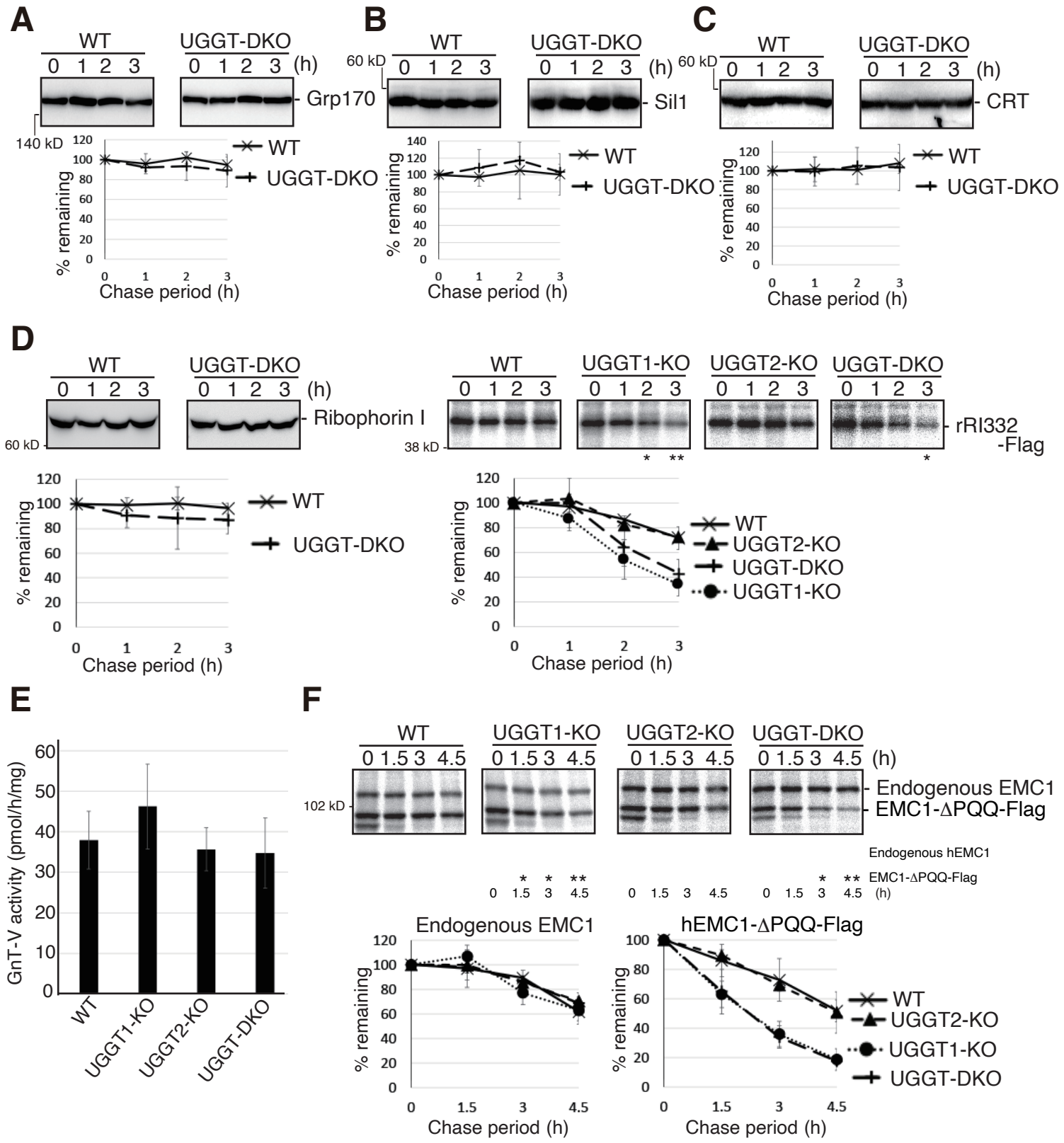
A
WT
UGGT-DKO
0 1 2 3
0 1 2 3 (h)
Grp170
140 kD
% remaining
Chase period (h)
WT
UGGT-DKO
B
60 kD
Sil1
C
CRT
D
Ribophorin I
60 kD
38 kD
UGGT1-KO
UGGT2-KO
rRI332
-Flag
E
GnT-V activity (pmol/h/mg)
F
102 kD
Endogenous EMC1
EMC1-ΔPQQ-Flag
Endogenous hEMC1
EMC1-ΔPQQ-Flag
0 1.5 3 4.5 (h)
hEMC1-ΔPQQ-Flag

Figure. 4

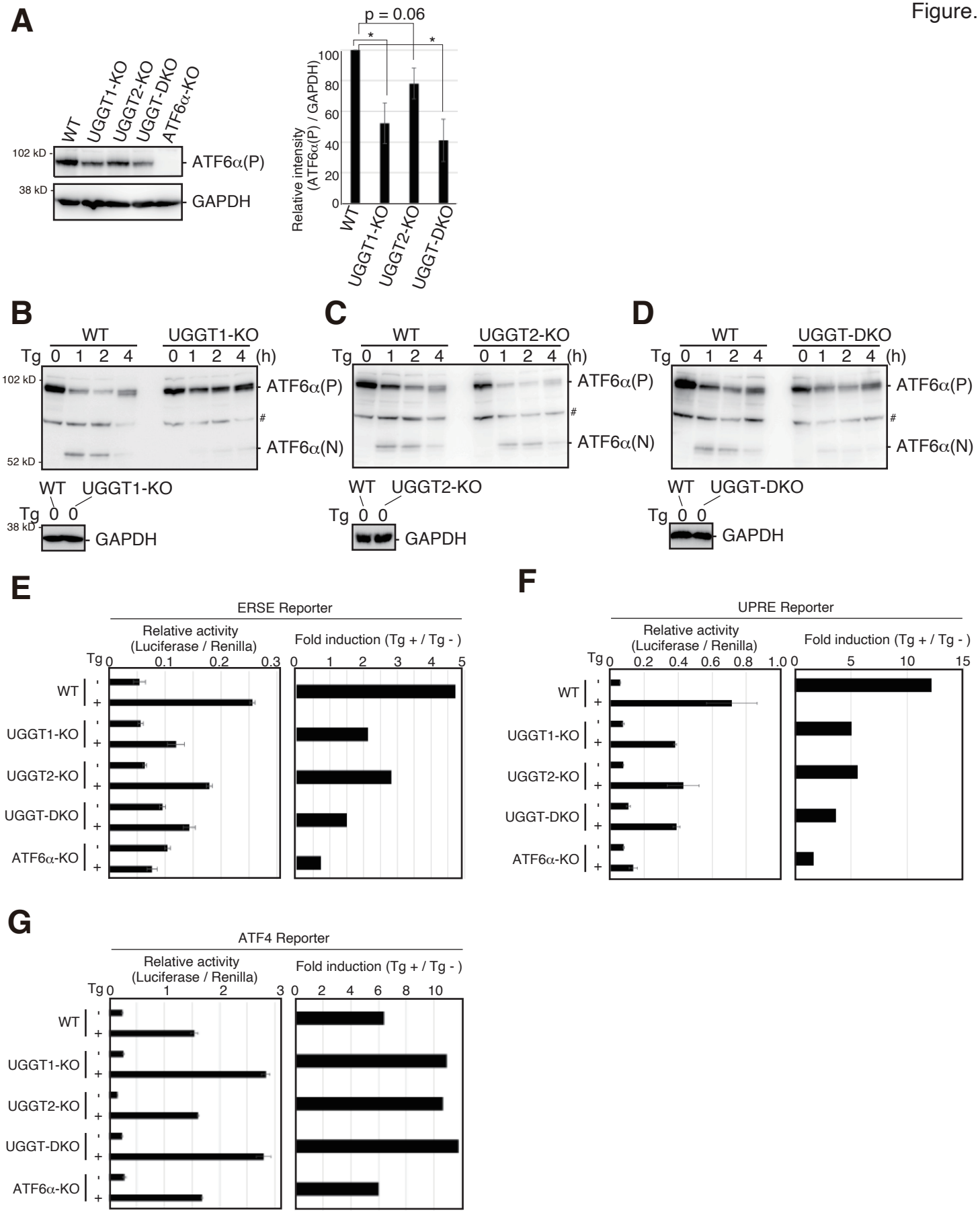
A
WT
UGGT1-KO
UGGT2-KO
UGGT-DKO
ATF6α-KO
102 kD
38 kD
ATF6α(P)
GAPDH
p = 0.06
*
*
Relative intensity (ATF6α(P) / GAPDH)
100
80
60
40
20
0
WT
UGGT1-KO
UGGT2-KO
UGGT-DKO
B
WT
UGGT1-KO
Tg 0 1 2 4 0 1 2 4 (h)
102 kD
52 kD
ATF6α(P)
#
ATF6α(N)
WT UGGT1-KO
Tg 0 0
38 kD
GAPDH
C
WT
UGGT2-KO
Tg 0 1 2 4 0 1 2 4 (h)
ATF6α(P)
#
ATF6α(N)
WT UGGT2-KO
Tg 0 0
GAPDH
D
WT
UGGT-DKO
Tg 0 1 2 4 0 1 2 4 (h)
ATF6α(P)
#
ATF6α(N)
WT UGGT-DKO
Tg 0 0
GAPDH
E
ERSE Reporter
Relative activity (Luciferase / Renilla)
Fold induction (Tg + / Tg -)
Tg
0 0.1 0.2 0.3
0 1 2 3 4 5
WT
UGGT1-KO
UGGT2-KO
UGGT-DKO
ATF6α-KO
F
UPRE Reporter
Relative activity (Luciferase / Renilla)
Fold induction (Tg + / Tg -)
Tg
0 0.2 0.4 0.6 0.8 1.0
0 5 10 15
WT
UGGT1-KO
UGGT2-KO
UGGT-DKO
ATF6α-KO
G
ATF4 Reporter
Relative activity (Luciferase / Renilla)
Fold induction (Tg + / Tg -)
Tg
0 1 2 3
0 2 4 6 8 10
WT
UGGT1-KO
UGGT2-KO
UGGT-DKO
ATF6α-KO

Figure 5

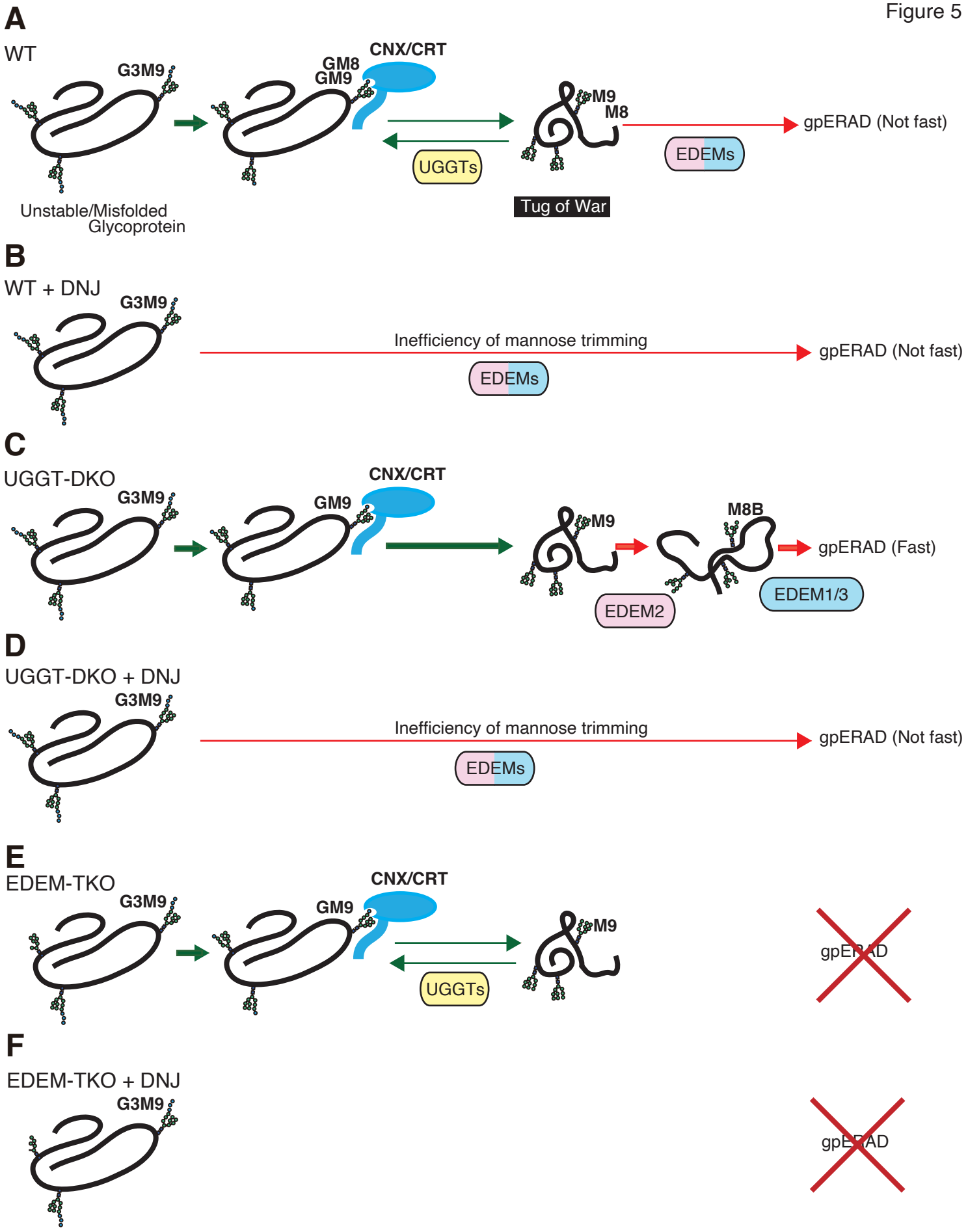
A
WT
G3M9
Unstable/Misfolded Glycoprotein
GM8
GM9
CNX/CRT
UGGTs
M9
M8
Tug of War
EDEMs
gpERAD (Not fast)
B
WT + DNJ
G3M9
Inefficiency of mannose trimming
EDEMs
gpERAD (Not fast)
C
UGGT-DKO
G3M9
GM9
CNX/CRT
M9
M8B
EDEM2
EDEM1/3
gpERAD (Fast)
D
UGGT-DKO + DNJ
G3M9
Inefficiency of mannose trimming
EDEMs
gpERAD (Not fast)
E
EDEM-TKO
G3M9
GM9
CNX/CRT
UGGTs
M9
gpERAD
F
EDEM-TKO + DNJ
G3M9
gpERAD

Figure 1
Figure supplement 1

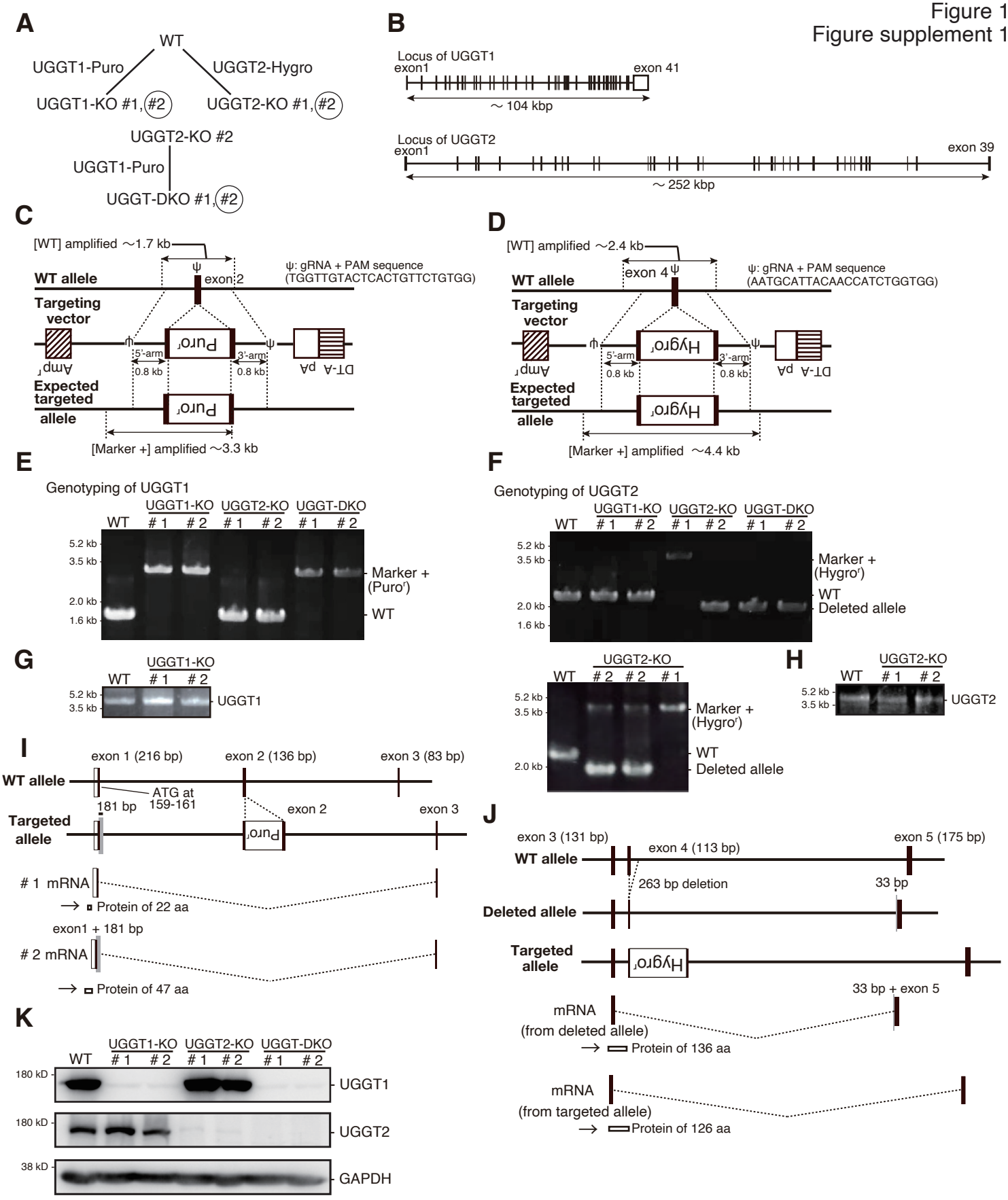

Genotype	Doubling Time (h)
WT	19.8
UGGT1-KO	21.5
UGGT2-KO	20.5
UGGT-DKO	20.0

Figure 1
Figure supplement 2

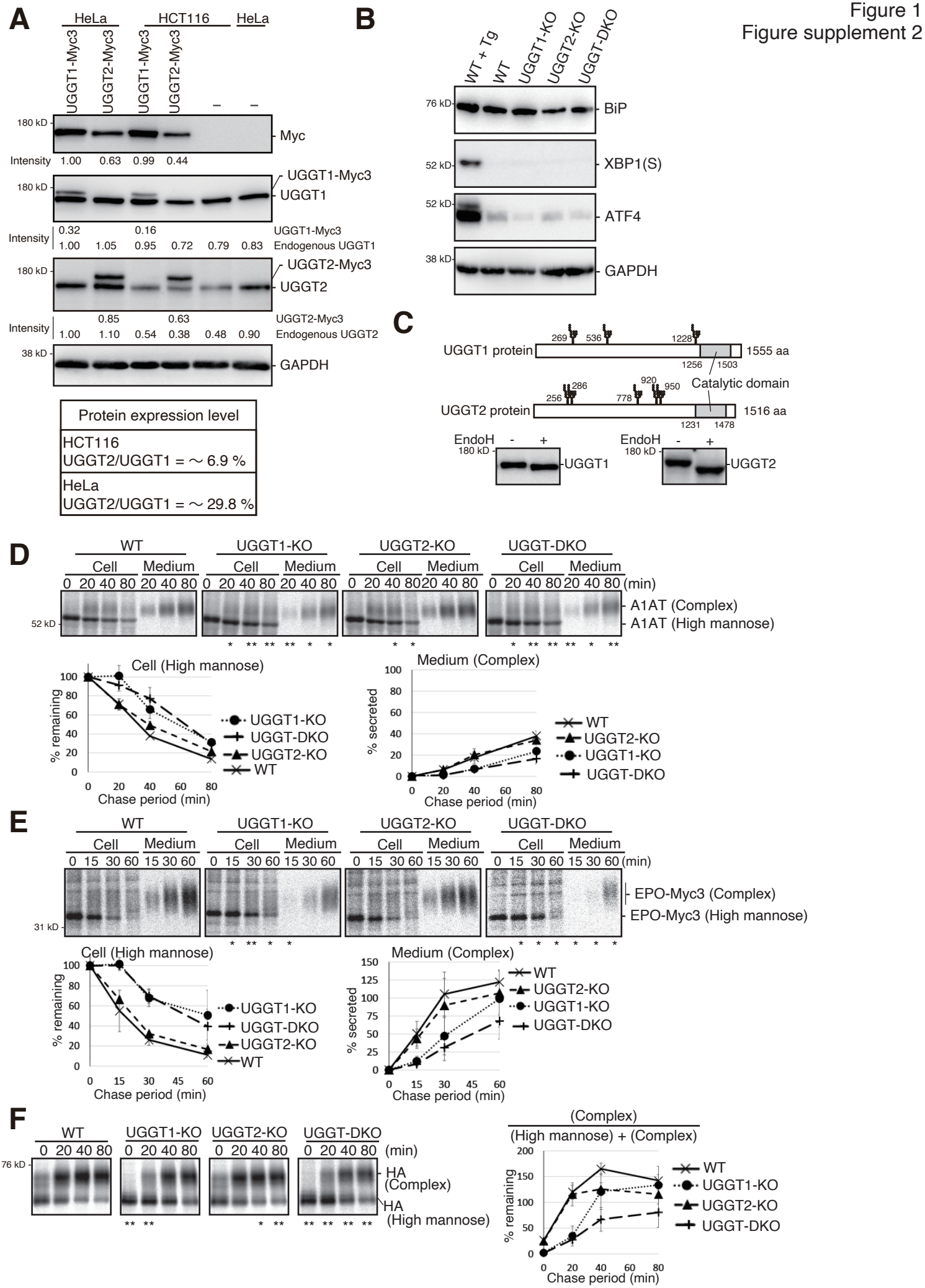

Figure 1
Figure supplement 3

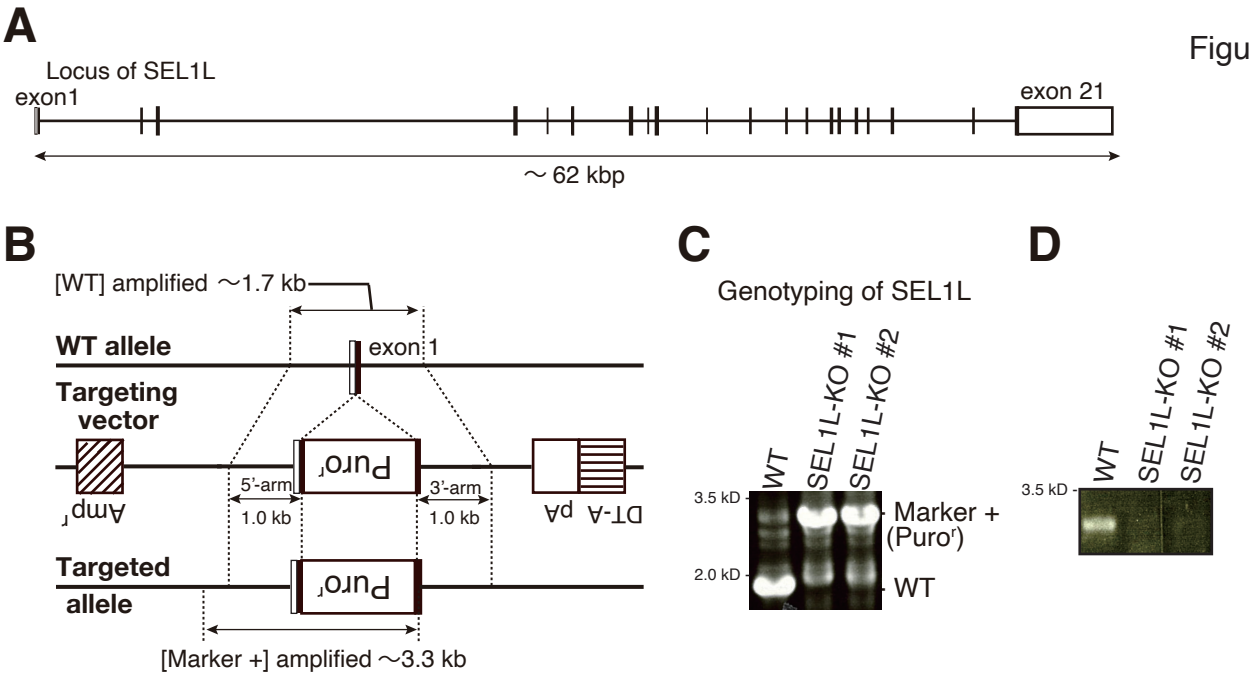

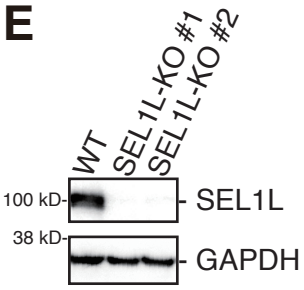

F

Genotype	Doubling Time (h)
WT	18.6
SEL1L-KO #1	19.3
SEL1L-KO #2	19.3

Figure 1
Figure supplement 4

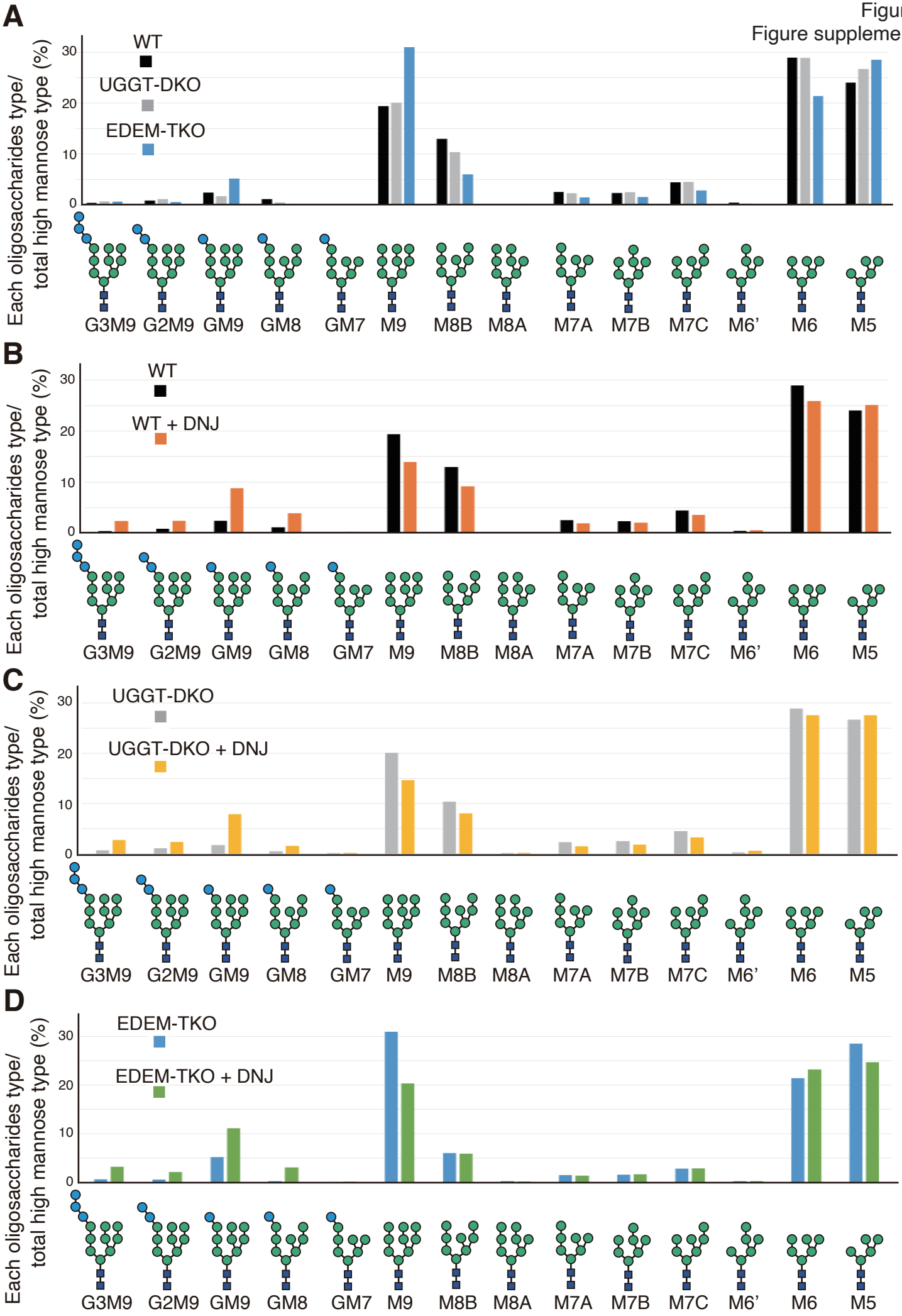

Figure. 3
Figure supplement 1

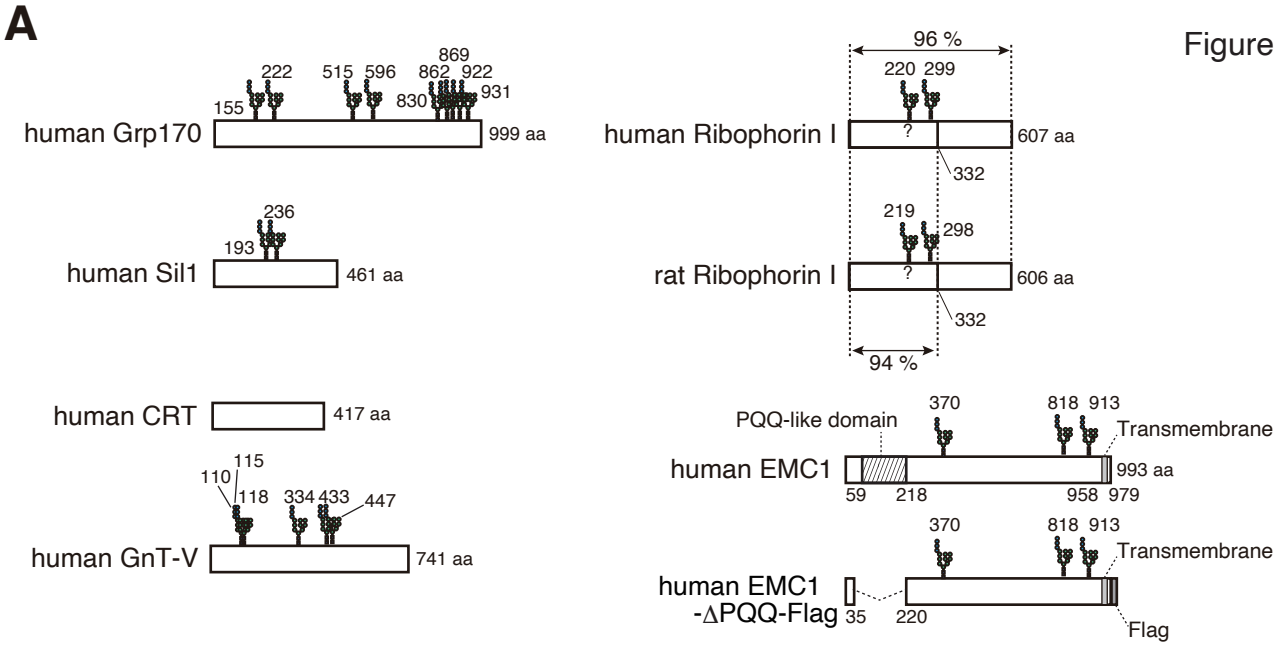

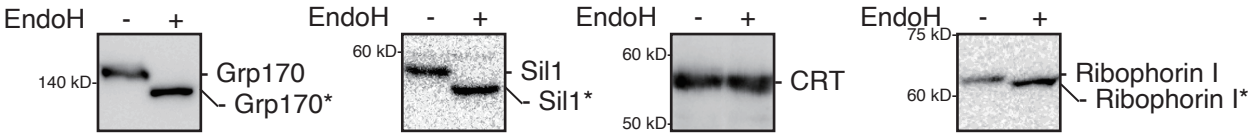
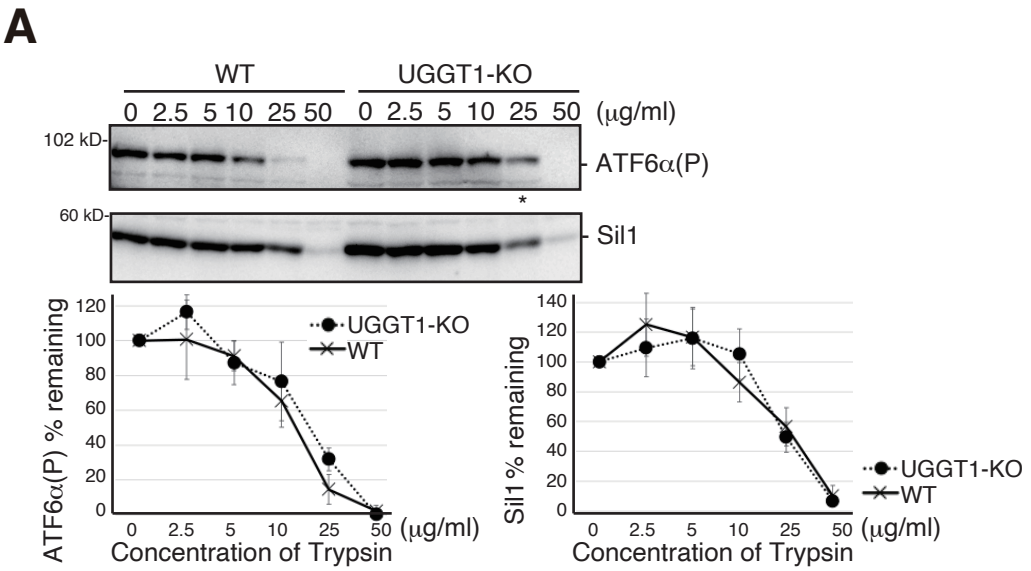
Figure 4
Figure supplement 1